



Fermi National Accelerator Laboratory

FERMILAB-Conf-98/213-E

CDF

Search for High Mass Photon Pairs in $p\bar{p}$ Collisions at $\sqrt{s} = 1.8$ TeV

Peter J. Wilson

For the CDF Collaboration

Fermi National Accelerator Laboratory

P.O. Box 500, Batavia, Illinois 60510

July 1998

Contributed Paper to the *29th International Conference on High-Energy Physics (ICHEP 98)*,
Vancouver, British Columbia, Canada, July 23-30, 1998

Disclaimer

This report was prepared as an account of work sponsored by an agency of the United States Government. Neither the United States Government nor any agency thereof, nor any of their employees, makes any warranty, expressed or implied, or assumes any legal liability or responsibility for the accuracy, completeness, or usefulness of any information, apparatus, product, or process disclosed, or represents that its use would not infringe privately owned rights. Reference herein to any specific commercial product, process, or service by trade name, trademark, manufacturer, or otherwise, does not necessarily constitute or imply its endorsement, recommendation, or favoring by the United States Government or any agency thereof. The views and opinions of authors expressed herein do not necessarily state or reflect those of the United States Government or any agency thereof.

Distribution

Approved for public release; further dissemination unlimited.

Search for High Mass Photon Pairs in $p\bar{p}$ Collisions at $\sqrt{s} = 1.8$ TeV

Abstract 675, Submitted to ICHEP 98, Vancouver, BC, July 1998

Peter J. Wilson

Fermi National Accelerator Laboratory

for the

CDF Collaboration

June 29, 1998

Abstract

We present results of a search for diphoton resonances produced inclusively and in association with a vector boson using 100 pb^{-1} of $p\bar{p}$ collisions using the CDF detector. We set upper limits on the product of cross section times branching ratio for $p\bar{p} \rightarrow \gamma\gamma + X$ and $p\bar{p} \rightarrow \gamma\gamma + W/Z$. Using a NLO prediction for associated production cross section of a Higgs with a vector boson (W or Z), we set an upper limit on the branching ratio for $H \rightarrow \gamma\gamma$. We set a lower limit on the mass of a ‘bosophilic’ Higgs boson (e.g. one which couples only to γ , W , and Z bosons with Standard Model couplings) of $82 \text{ GeV}/c^2$ at 95% C.L.

Introduction

Many processes in extensions of the Standard Model (SM) result in final-state signatures involving two vector gauge bosons, $VV + X$, where V is either a W , Z , or photon. The photon is the lightest of these, and also has the advantage to the experimentalist that it is stable and hence does not decay into many different final states. The production of very massive photon pairs ($M_{\gamma\gamma} > 150 \text{ GeV}/c^2$) in 1.8 GeV $p\bar{p}$ collisions is calculable in the Standard Model, and is small compared to the cross-sections for producing new states via quark-antiquark annihilation, making this an attractive channel in which to search for new particles or interactions. Examples of possible sources of high mass diphoton pairs are a new interaction at a high scale manifesting itself as a $q\bar{q}\gamma\gamma$ contact interaction[1], a ‘bosophilic’ Higgs[2, 3, 4, 5], or a heavy analog of the π^0 that also does not couple to fermions[6]. In this paper we focus on a Higgs decaying to two photons.

The total $p\bar{p}$ production cross section for a SM Higgs boson is approximately 3 pb for $M_H = 80 \text{ GeV}/c^2$ [7] which is dominated by the gluon-gluon fusion process. At this mass the decay is dominated by $H \rightarrow b\bar{b}$ with the branching ratio to $\gamma\gamma$ on the order of 10^{-4} . Some extended models introduce anomalous couplings[8] or additional Higgs multiplets [3, 5] enhancing the coupling to photons or suppressing the coupling to fermions. The result is a low mass Higgs with significantly increased branching fraction to two photons. In the bosophilic models, the coupling to fermions at tree level is shut off while maintaining the SM coupling to vector bosons. Although the decay to two photons requires a loop, it is the dominant decay for $M_H < M_W$. For $M_H > M_W$ the decay $H \rightarrow WW^*$ becomes dominant. Since the bosophilic Higgs has no SU(3) coupling the gluon-gluon fusion production mechanism is lost and the dominant production mode in $p\bar{p}$ collisions at $\sqrt{s} = 1.8 \text{ TeV}$ is associated production with a W or Z boson. For $M_H = 80 \text{ GeV}/c^2$ the total associated production cross section is about 0.8 pb. The most stringent limits on bosophilic Higgs have been set by $D\bar{O}$ with a lower limit of $81 \text{ GeV}/c^2$ at 95% C.L.[9] and OPAL with a limit of $76.5 \text{ GeV}/c^2$ at 95% C.L.[10]. These previous limits and the limit set in this paper all use the branching ratios of reference [3].

In this paper we describe a search for departures from SM expectations for inclusive high-mass $\gamma\gamma$ production and $\gamma\gamma$ production in association with a W or Z boson. This search uses $100 \pm 8 \text{ pb}^{-1}$ of data collected between 1992 and 1995 with the Collider Detector at Fermilab (CDF). The photon selection criteria for this analysis were optimized to remain efficient for very high energy photons. The analysis is complimentary to the previous diphoton cross section analysis[11], in which very strict photon selection requirements are used to reduce the large jet fake backgrounds maximizing signal significance, but which become progressively less efficient with E_T for high E_T ($> 50 \text{ GeV}$) photons. It is also complimentary to the recent diphoton + X search analysis[12] which was focused on non-resonant diphoton signatures such as gauge mediated SUSY.

CDF Detector

We briefly describe the CDF detector which is described in great detail elsewhere[13]. The magnetic spectrometer consists of three tracking devices immersed in the 1.4 T field of a 3 m diameter 5 m long super-conducting solenoid. The magnetic field and three tracking devices are all arranged with their principal axis parallel to the proton beam direction (z -axis)[14]. The tracking device closest to the beam line is a four-layer silicon micro-strip vertex detector (SVX), used to find secondary vertices, with layer radii between 2.8 cm and 7.9 cm[15]. Surrounding the SVX is a set of time projection chambers (VTX) which identifies the $p\bar{p}$ interaction(s) with a series of $r - z$ measurements out to a radius of 22 cm. The central tracking chamber (CTC) is a 3.5 m long 84 layer drift chamber surrounding the VTX. The CTC wires, ranging in radius from 31.0 cm to 132.5 cm, are arranged in 4 superlayers of axial wires alternating with 3 superlayers of stereo wires. The calorimeter, which is constructed in projective

electromagnetic and hadronic towers, consists of the central barrel ($|\eta| < 1.1$) which surrounds the solenoid, the end-plugs ($1.1 < |\eta| < 2.4$) which form the magnet poles and the forward ($2.4 < |\eta| < 4.2$). Wire chambers with cathode strip readout (CES) are located at shower maximum in the central electromagnetic calorimeter. These chambers provide a two dimensional shower profile which is used to discriminate on a statistical basis between photons and π^0 backgrounds. Additional statistical discrimination is provided by difference in conversion probability for photon/ π^0 in the 1 radiation length of the coil. The presence of a conversion is detected using wire chambers located between the coil and the central calorimeter (CPR). The central muon chambers ($|\eta| < 1.1$) are located outside central calorimeter to detect particles penetrating at least 5 interaction lengths of material.

Di-Photon Event Selection

Photons are identified as a narrow shower in the electromagnetic calorimeter with no associated high P_T charged particle track. The energy in the hadronic calorimeter and adjoining regions of the electromagnetic calorimeter must be small to reject jet backgrounds. For high E_T photons there is a background from $\pi^0 \rightarrow \gamma\gamma$ decays where both photons are in the same calorimeter tower.

The candidate $\gamma\gamma$ events must pass the diphoton requirements of the three-level CDF trigger. The first hardware level requires two central electromagnetic calorimeter trigger towers with $E_T > 4$ GeV. The second hardware level requires two central electromagnetic clusters with $E_T > 16$ GeV and a loose cut on the hadronic energy: $E_T(HAD)/E_T(EM) < 0.125$. In the third trigger level, the cluster is found using the offline reconstruction algorithm and the 16 GeV threshold is repeated.

Offline event selection requires at least two central electromagnetic clusters each satisfying the following requirements: $E_T > 22$ GeV, no track pointing at the cluster (or one track with $P_T < 1$ GeV/c), pulse height and cluster shape in the CES consistent with a photon (to reject π^0 and cosmics), no additional CES cluster in the same 15° azimuthal section of the calorimeter (to reject π^0), and minimal energy deposited in the hadronic calorimeter towers behind the cluster. Isolation requirements based on track and calorimeter activity in an $\eta - \phi$ cone, with radius $\Delta R \equiv \sqrt{(\Delta\phi)^2 + (\Delta\eta)^2} = 0.4$, around the cluster are used to reduce backgrounds from jets: $\Sigma P_T(Tracks) < 5.0$ GeV and $(E_T(\Delta R < 0.4) - E_T(Cluster)) < 2.0$ GeV. The calorimeter isolation energy is corrected for leakage from the cluster and for pile-up from multiple interactions. There must also be at least one reconstructed primary vertex which satisfies $|z_{VERTEX}| < 60$ cm and all energy measured in the central hadronic calorimeters is required to be in time with the collision. These last two requirements reject backgrounds from cosmic rays. Figure 1 shows the invariant mass distribution of 287 diphoton candidate events passing these selection criteria. The efficiency to find an isolated photon is measured using a control sample of electrons from Z^0 decay to be $84 \pm 4\%$. The combined diphoton and event selection efficiencies is $63 \pm 6\%$.

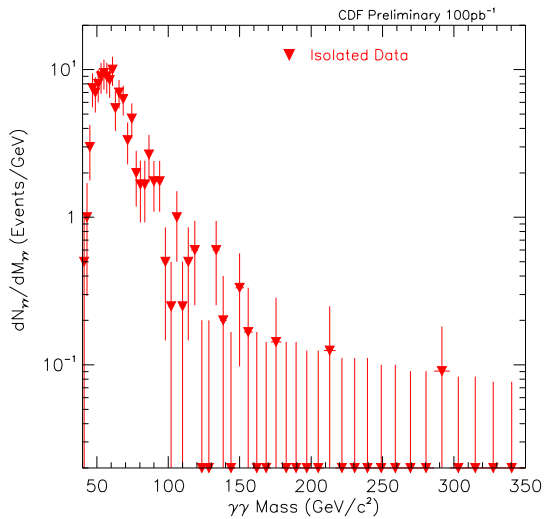


Figure 1: Diphoton candidate invariant mass distribution (287 events) with a binwidth of 2 times the mass resolution (σ).

Backgrounds

The dominant backgrounds for this analysis are γ -jet and jet-jet production, where the jets have faked photons by fluctuating to a single π^0 or η , and real photon pairs from prompt QCD production. The background from $Z^0 \rightarrow e^+e^-$ with both electrons faking photons is less than 1 event. The jet fake rate is measured directly from the data. For clusters with $E_T < 35$ GeV, the lateral shape of the shower in the CES system is used to discriminate between prompt photons and photons from $\pi^0 \rightarrow \gamma\gamma$. Above 35 GeV, where the CES shapes from photons and π^0 s are indistinguishable, the conversion probability in advance of the CPR chambers is used to measure the photon purity[17]. In the diphoton candidate sample, 183 ± 56 events are from jet fakes and 104 ± 55 events are from real photon pairs for a background fraction of $64 \pm 19\%$. The mass spectrum of the jet fakes is determined using a fakes rich control sample consisting of events passing all of the photon selection requirements above except that one or both clusters fail the calorimeter isolation requirement. The mass distribution of the 198 event fakes rich sample is normalized to the number of fakes measured in the diphoton candidate sample (183 events).

Two Standard Model processes make significant contributions to prompt diphoton production: $q\bar{q} \rightarrow \gamma\gamma$ and $gg \rightarrow \gamma\gamma$. In addition, initial and final state radiation from γ -jet production contributes indirectly to the diphoton mass

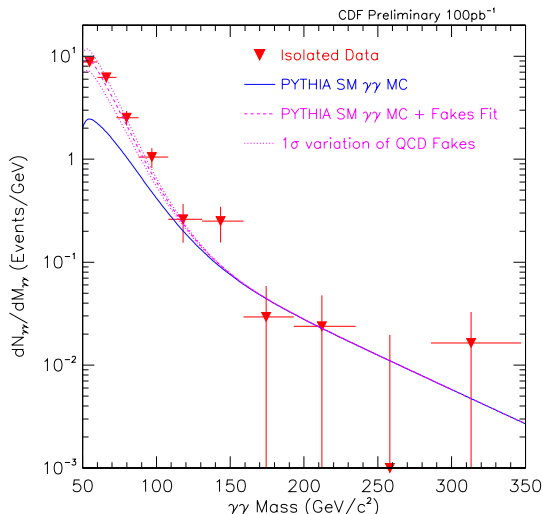


Figure 2: The diphoton mass distribution is compared with background predictions with a binning of about 10 times the mass resolution.

spectrum. In the indirect case, several processes contribute to the γ -jet production: $q\bar{q} \rightarrow \gamma g$, $qg \rightarrow q\gamma$, and $q\bar{q} \rightarrow g\gamma$. These Standard Model processes are modeled using PYTHIA 6.1 with CTEQ4L structure functions and run through the CDF fast detector simulation. Figure 2 shows a comparison of the diphoton mass spectrum for the 287 isolated diphoton candidates (triangles) with background predictions. The solid line is the Standard Model diphoton prediction from PYTHIA Monte Carlo, the dashed line is the sum of the PYTHIA diphoton and the jet fakes prediction, and the dotted lines represent 1σ uncertainties on the fakes estimate. The total predicted background from fakes plus QCD diphoton production is 313 ± 69 events. The data is well modeled by the background predictions: above $150 \text{ GeV}/c^2$ we observe 5 events compared to a background prediction of 4.5 ± 0.6 events

Limit on Inclusive $\gamma\gamma$ Production

We set limits on the cross section for diphotons with $M_{\gamma\gamma} > 100 \text{ GeV}/c^2$. The acceptance for diphoton production is evaluated using $H^0 \rightarrow \gamma\gamma$ as a model for a heavy new particle. The Higgs Monte Carlo is generated using PYTHIA, simulated using the CDF fast detector simulation and passed through the same event selection criteria as the data. The acceptance times efficiency increases linearly from 10.5% at $100 \text{ GeV}/c^2$ to 14.4% at $300 \text{ GeV}/c^2$. We set 95% C.L.

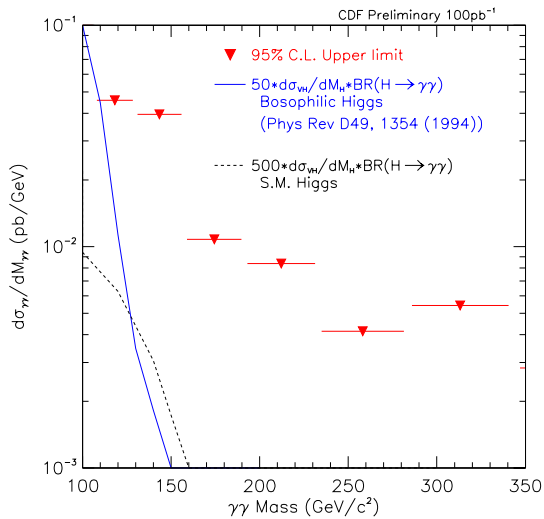


Figure 3: Cross section limit for high mass diphoton production.

upper limits for the cross section in each mass bin assuming all events are signal with no background or Standard Model subtraction. The cross section limit in each bin is given by the following expression:

$$\sigma(p\bar{p} \rightarrow \gamma\gamma) < \frac{N^{95\% \text{ CL}}(\gamma\gamma)}{\epsilon \cdot A \cdot \int \mathcal{L} dt} \quad (1)$$

where $N^{95\% \text{ CL}}(\gamma\gamma)$ is the 95% CL upper limit on the number of diphotons in the mass bin, ϵ is the selection efficiency, A is the acceptance and $\int \mathcal{L} dt$ is the integrated luminosity. The upper limit on the number of events in each bin is determined, including systematic uncertainties, using the method of reference [18]. The total systematic uncertainty of 13% consists of 8% from the luminosity measurement, 10% uncertainty on the selection efficiencies and 3% uncertainty from the acceptance.

Figure 3 shows the cross section limit in six mass bins above 100 GeV/c². For comparison the cross section times branching fraction for $p\bar{p} \rightarrow H^0 + W/Z \rightarrow \gamma\gamma + X$ production is shown multiplied by 500 for SM branching fractions (dashed curve) and by 50 for bosophilic branching fractions (solid curve)[3].

Selecting $\gamma\gamma + W/Z$ Candidates

The inclusive $\gamma\gamma$ analysis is not sensitive to production of Higgs decaying to two photons in the mass region 60-100 GeV/ c^2 because the backgrounds from jet fakes and QCD di-photon production are too high. To increase sensitivity we concentrate the analysis on the signature $\gamma\gamma + W/Z$. The additional requirement of a W or Z boson significantly reduces the backgrounds from Jet fakes and QCD $\gamma\gamma$ production. To achieve a high acceptance for all W and Z decay channels, the vector bosons are selected using simple signatures which yield significant background reductions without the inefficiency of full reconstruction. The backgrounds from jet fakes and QCD $\gamma\gamma$ production were evaluated using the fakes control sample and PYTHIA Monte Carlo used in the inclusive $\gamma\gamma$ analysis. Backgrounds from Electroweak processes were found to be insignificant.

The vector boson selection consists of the logical OR of three general categories based on decay channels as follows:

1. Central Isolated electron ($E_T > 20$ GeV) or muon ($P_T > 20$ GeV/ c) for $W \rightarrow l\nu$ and $Z^0 \rightarrow l^+l^-$, OR
2. $\cancel{E}_T > 20$ GeV for $W \rightarrow l\nu$ and $Z^0 \rightarrow \nu\nu$, OR
3. Two Jets ($E_T > 15$ GeV, $|\eta| < 2.0$) for $W \rightarrow qq'$ and $Z^0 \rightarrow q\bar{q}$.

The leptons are selected using the isolated central lepton requirements of the top lepton-plus-jets analyses[16]. The lepton identification efficiencies are measured in data samples of Z bosons decaying to electrons ($77.8 \pm 0.6\%$) and muons ($90.6 \pm 0.5\%$). The missing E_T is corrected for any high P_T central muons. Since mismeasured jet energies can result in false \cancel{E}_T , events with any jet ($E_T^{\text{jet}} > 10$ GeV) within 25° of the missing E_T direction are rejected. Jets are identified in the calorimeter using a fixed cone algorithm with a cone size $\Delta R = 0.4$. Any jet near an electron ($\Delta R(\text{Jet} - e) < 0.4$) or photon ($\Delta R(\text{Jet} - \gamma) < 0.6$) is ignored. Finally the jet-jet invariant mass is required to be consistent with a W or Z boson: $40 < M_{JJ} < 130$ GeV/ c^2 .

The event selection is summarized in Table 1 including the number of events passing for the diphoton candidate sample and the combined background estimates. The final sample consists of 6 events compared to a predicted background of 6.2 ± 2.1 events. One event passes both the jet-jet and the \cancel{E}_T selection requirements; another event has a $\gamma\gamma$ invariant mass of 137 GeV/ c^2 and $\cancel{E}_T = 21$ GeV. The total of all electroweak backgrounds is 0.2 ± 0.2 events. Figure 4 shows the $\gamma\gamma$ mass distribution, before and after the combined vector selection requirements, for the isolated diphoton data and the background samples. There is no evidence of a $\gamma\gamma$ resonance in the data.

Selection	Isolated Sample	Background Estimate
Two Isolated Photons $E_T^\gamma > 22$ GeV	287	313 ± 69
<i>W/Z Selection:</i>		
Central Electron, $E_T > 20$ GeV	1	0
Central Muon, $P_T > 20$ GeV	0	0
$\cancel{E}_T > 20$	3	1.8 ± 1.3
2 Jets ($E_T > 15$, $40 < M_{JJ} < 130$ GeV/ c^2)	3	4.6 ± 1.9
Any <i>W/Z</i> signature	6	6.2 ± 2.1

Table 1: Summary of Event Selection including number of data events and estimate of QCD backgrounds from fakes (non-isolated control sample) plus SM $\gamma\gamma$.

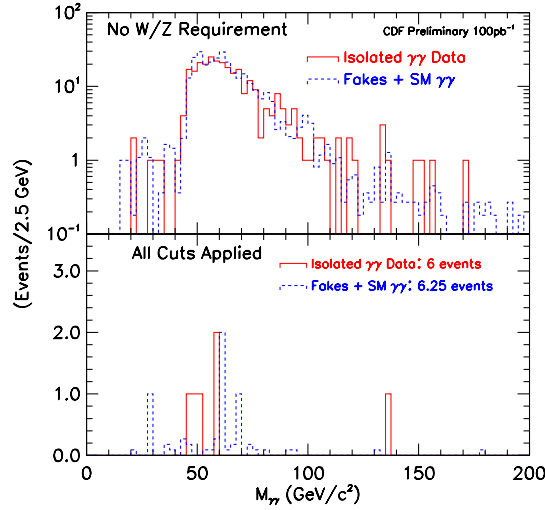


Figure 4: Photon-photon mass distribution with photon selection cuts only (top) and after *W/Z* selection cuts (bottom).

Limits on $\gamma\gamma + W/Z$ Production

We set an upper limit on the cross section times branching ratio for the process $p\bar{p} \rightarrow W/Z + \gamma\gamma$ as a function of $\gamma\gamma$ mass:

$$\sigma(p\bar{p} \rightarrow W/Z + \gamma\gamma) < \frac{N^{95\%CL}(W/Z + \gamma\gamma)}{\epsilon \cdot A \cdot \int \mathcal{L} dt} \quad (2)$$

Where $N^{95\%CL}(W/Z + \gamma\gamma)$ is the upper limit on the number of events, $\epsilon \cdot A$ is the product of efficiency times acceptance, and $\int \mathcal{L} dt$ is the integrated luminosity. The number of signal events at each mass is taken as the number of isolated diphoton events passing the vector (W/Z) selection cuts and falling within a $\pm 3\sigma(M_H)$ mass window around the candidate mass. We calculate $N^{95\%CL}$, the 95% C.L. upper limit on the number of events at each mass, assuming no background subtraction and including a Gaussian systematic uncertainty of 17% which includes photon selection efficiency (10%), luminosity (8%), gluon radiation modeling (11%), and jet energy scale (7%).

The acceptance is determined from Monte Carlo samples of associated Higgs + W/Z generated with PYTHIA 6.1 and CTEQ4L structure functions. Figure 5 shows the product of the efficiency times acceptance as a function of M_H before and after the vector boson selection cuts. The efficiency times acceptance increases from about 4% for $M_H = 60 \text{ GeV}/c^2$ to about 9% for $M_H > 100 \text{ GeV}/c^2$. The mass dependence of the acceptance is dominated by the photon E_T requirement.

Figure 6 shows the 95% C.L. upper limit on the cross section times branching ratio for $p\bar{p} \rightarrow W/Z\gamma\gamma$. The overlaid dashed curve is the prediction for a bosophilic Higgs using the branching ratios from reference [3] and a NLO cross section calculation from reference [7] using the CTEQ4M structure functions. A 95% C.L. lower limit on the mass of a bosophilic Higgs is set at $82 \text{ GeV}/c^2$.

An upper limit on the branching fraction for $H \rightarrow \gamma\gamma$ is obtained by dividing the cross section limit on $W/Z + \gamma\gamma$ by the predicted cross section for $W/Z + H$ production. The resulting branching ratio upper limit is shown in Figure 7 along with the published upper limit from OPAL[10]. The overlaid dashed and dotted curves are the bosophilic and Standard Model (scaled up by a factor of 100) branching ratio predictions.

Conclusions

We have presented results of searches for massive diphoton production both inclusively and in association with a high P_T lepton, \cancel{E}_T , or dijets. The latter channels are sensitive to production of a vector boson in association with Higgs boson which subsequently decays to photons. Both the inclusive and exclusive signatures are consistent with predictions from SM sources. We set an upper limit on the cross section times branching fraction for $p\bar{p} \rightarrow \gamma\gamma + W/Z$ between 60 and $160 \text{ GeV}/c^2$. Using a NLO calculation of the SM cross section for

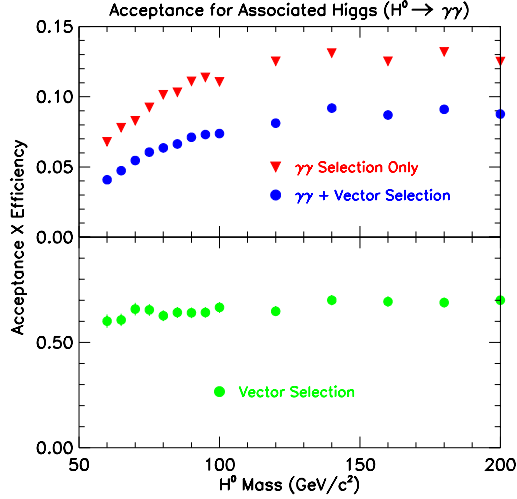


Figure 5: Acceptance times efficiency for VH production where the W and Z decay via any SM decay and the Higgs decays to $\gamma\gamma$.

$p\bar{p} \rightarrow VH$ we set a 95% C.L. upper limit on the branching fraction for $H \rightarrow \gamma\gamma$. Between approximately 60 and 100 GeV/c^2 the upper limit on the branching fraction is less than 1. Using the branching ratios of reference [3] the lower limit on the mass of a bosophilic Higgs is 82 GeV/c^2 at 95% C.L.

Acknowledgments

We thank the Fermilab staff and the technical staffs of the participating institutions for their vital contributions. This work was supported by the U.S. Department of Energy and National Science Foundation; the Italian Istituto Nazionale di Fisica Nucleare; the Ministry of Education, Science and Culture of Japan; the Natural Sciences and Engineering Research Council of Canada; the National Science Council of the Republic of China; the Swiss National Science Foundation; and the A.P. Sloan Foundation.

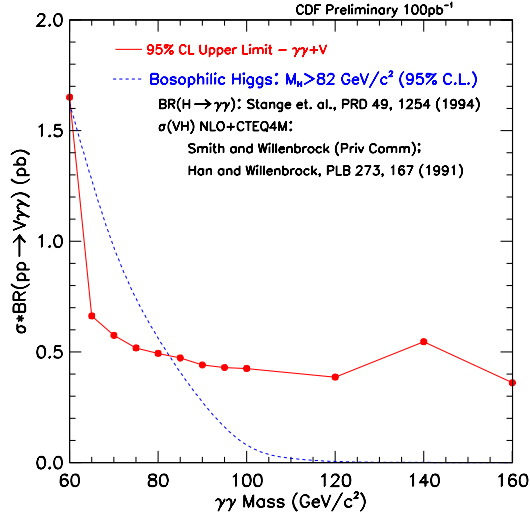


Figure 6: Upper limit on the $\gamma\gamma + W/Z$ cross section as a function of $\gamma\gamma$ mass.

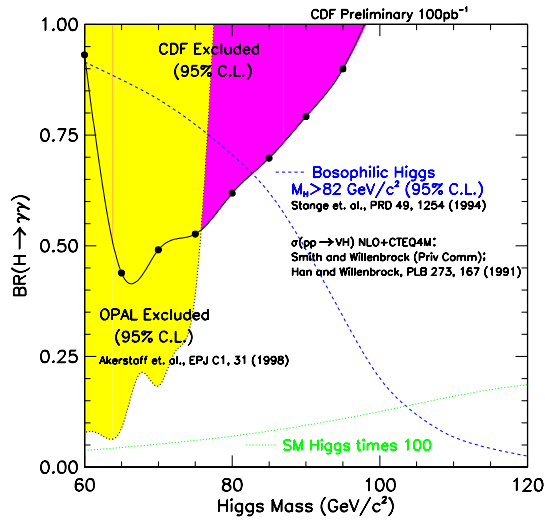


Figure 7: Upper limit on the branching fraction for $H \rightarrow \gamma\gamma$ assuming Standard Model production cross section for $W/Z + H$ (shaded above solid curve). Also shown is the published OPAL limit (light shaded region above dotted curve).

References

- [1] T.G. Rizzo, Phys. Rev. **D51**, 1064 (1995).
- [2] H. Haber, G. Kane, and T. Sterling, Nucl. Phys. **B161**, 493 (1979).
- [3] A. Stange, W. Marciano, and S. Willenbrock, Phys. Rev. **D49**, 1354 (1994).
- [4] M.G. Diaz and T. Weiler, preprint VAND-TH-94-1 (1994) (hep-ph/9401259).
- [5] A.G. Akeroyd, Phys. Lett. **B368**, 89 (1996).
- [6] K. Lane, Phys. Lett. **B357**, 624 (1995).
- [7] M. Smith and S. Willenbrock private communication; T. Han and S. Willenbrock, Phys. Lett. **B273**, 167 (1991).
- [8] M.C. Gonzalez-Garcia, S.M. Lietti, and S.F. Novaes, Phys. Rev. **D57**, 7045 (1998).
- [9] D0 Collab., submitted to the XVII International Symposium on Lepton Photon Interactions (1997).
<http://d0sgio.fnal.gov/public/new/conferences/lp97.html>
- [10] K. Ackerstaff *et al.*, Eur. Phys. J. **C 1**, 31 (1998).
- [11] F. Abe *et al.*, Phys. Rev. Lett. **70**, 2232 (1993).
- [12] A. Abe *et al.*, hep-ex/9801019. Submitted to Phys. Rev. Lett.
- [13] F. Abe *et al.*, Nucl. Instrum. Methods, **A271**, 387 (1988).
- [14] The z (longitudinal) axis is along the proton beam axis; r is the transverse coordinate. Pseudorapidity (η) is $\eta \equiv -\ln(\tan(\theta/2))$, where θ is the polar angle. Transverse energy is defined as $E_T = E \sin \theta$.
- [15] D. Amidei *et al.*, Nucl. Instrum. Methods, **A350**, 73 (1994).
- [16] F. Abe *et al.*, Phys. Rev. D **50**, 2966 (1994) and F. Abe *et al.*, Phys. Rev. Lett. **73**, 2662 (1994).
- [17] F. Abe *et al.*, Phys. Rev. Lett. **73**, 1662 (1994).
- [18] R.D. Cousins and V.L. Highland, Nucl. Instrum. Meth. **A320**, 331 (1992); equation 17b: $U_n = U_{n0}[1 + E_n(\sigma_r^2/2)\{1 + (E_n\sigma_r^2/2)^2\}]$.